ISOCAM LW Channel Field of View Distortion. Version 0.9

Uncomplete Draft

Hervé Aussel

Service d'Astrophysique, CE-Saclay, F-91191 Gif-sur-Yvette Cedex, France
aussel@discovery.saclay.cea.fr

August 13, 1998

Contents

Introduction

Field distortion is an image aberration that affects the scale of the objects. In ISOCAM, distortion is due to the off-axis Fabry mirrors that direct the light beam toward the various detectors. It has been measured during the pre-launch calibration phase, using the simulator installed at IAS, Orsay. These measurements were done before the integration of ISOCAM into the satellite. Therefore, flight measurements need to be performed, because the optical configuration of the system { instrument + telescope } might be different from the one simulated on the ground.

This report consist in two parts : a general description on how can ISOCAM LW channel be measured and corrected, and the detailed decription of the performed measurments in appendix. Readers wondering about how to take distortion into account, just can read the first part, or even section 3. However, appendix will be worth for people interested in getting a feeling of what are the possibilities of the technique.

In a first section,I will briefly recall the properties of the distortion, and examine methods to measure it with flight observations. Since all envisionned method demand to accurately measure the position of a point source on ISOCAM array, a second part will describe the methods that can be used for this task. In a third part, we will explain how distortion can be corrected.

1 Field of view distortion measurement.

The distortion of field of view is a well known optical defect, often encounterd in astronomy. We will define it, in order to derive some hypothesis that will allow to measure it.

1.1 Image aberrations.

Images of telescope suffer from various aberrations, that were classified by von Seidel [Ruten & van Verrooij, 1988], [Lena, 1988], for the monochromatic ones. They are listed in table 1. Four of them affect the sharpness of the image. This means that the image of a point source is not a point, but that it is more or less blurred [1]. The last one, the distortion, affect the scale of the image: point source images are points, but extended images are deformed.

In ISOCAM, the resolution being rather low, the loosing of sharpness is not very important. These effect could be investigated by comparing the PSF shape when they are measured at various position of the array. No striking difference has been found at the present time.

At first order, it seem to be a reasonable hypothesis that the aberration of ISOCAM are dominated by pure field distortion, as it will be explained in next section.

1.2 Field of view distortion

The principle of distortion is illustrated by figure 1, taken from [Ruten & van Verrooij, 1988]. We can note on the top pannel that all rays focus on the focal plane in a single point: this

[1] This definition is based, of course, on optical geometry, without taking diffraction into account.

name	type	affect	deformation
spherical aberration	axial	sharpness	focal lenght varies with distance to optical axis.
coma	off axis	sharpness	focal length varies sitance to axis.
astigmatism	off axis	sharpness	the focal length of the instrument varies with direction.
field curvature	off axis	sharpness	focal surface not planar
distortion	off axis	scale	image is not homothetic to object, except for point sources.

Table 1: the 5 monochromatic image aberrations as classified by von Seidel (1850).

explain why the sharpness of the image is not modified, the image of a point source being a point source. The deformation comes from the fact that the rays do not focus on the line parallel to the incoming rays that go trought the optical center of the system (dashed line).

The principal source of the distortion aberration are off axis mirrors and off axis pupils. They are present in the optical system {ISO + ISOCAM}, since the Fabry mirror, that allows for selecting between the LW and SW channels, is cylindrical.

Field distortion being an off axis effect, the aberration is equal to zero on the optical axis. This means that an image of a star at the center of the array is not distorded, and can be use as a reference. Point sources at the edges of the array will be displaced with respect to their real position in the sky. Moreover, the area of sky seen by a pixel at the edges of the array will be different from the area seen by the pixel on the optical axis.

The light beam crosses the filter and the lens before arriving on the detector. These optic component can add some aberrations to the image. Three effects can be added :

1. displacement of the image since the filters are tilted and since the lens position is not well defined (lens jitter).

2. achromatic image aberrations due to the lens and filters.

3. chromatic image aberrations due to the lens and filters.

All this points have to be investigated carefully. This is only possible by measuring distortion for a wide range of optical configurations. If the third point (chromatism) could be neglected, the number of configurations would strongly decrease, since we could only probe a broad band filter (representative for all tilded filter), and a CVF position (CVF filters are not tilted), for each lens and fabry configuration. The LW channel lens are in Germanium. The optical properties of this material have been investigated by [Icenogle et al., 1976]. They report that its refractive index n decrease by less than 1.5% at 94 K from 3 to 12 μm, and that $\Delta n/\Delta T \sim 3.10^4 K^{-1}$. This could indicate that chromatism might be low, but this has to be checked in real observations.

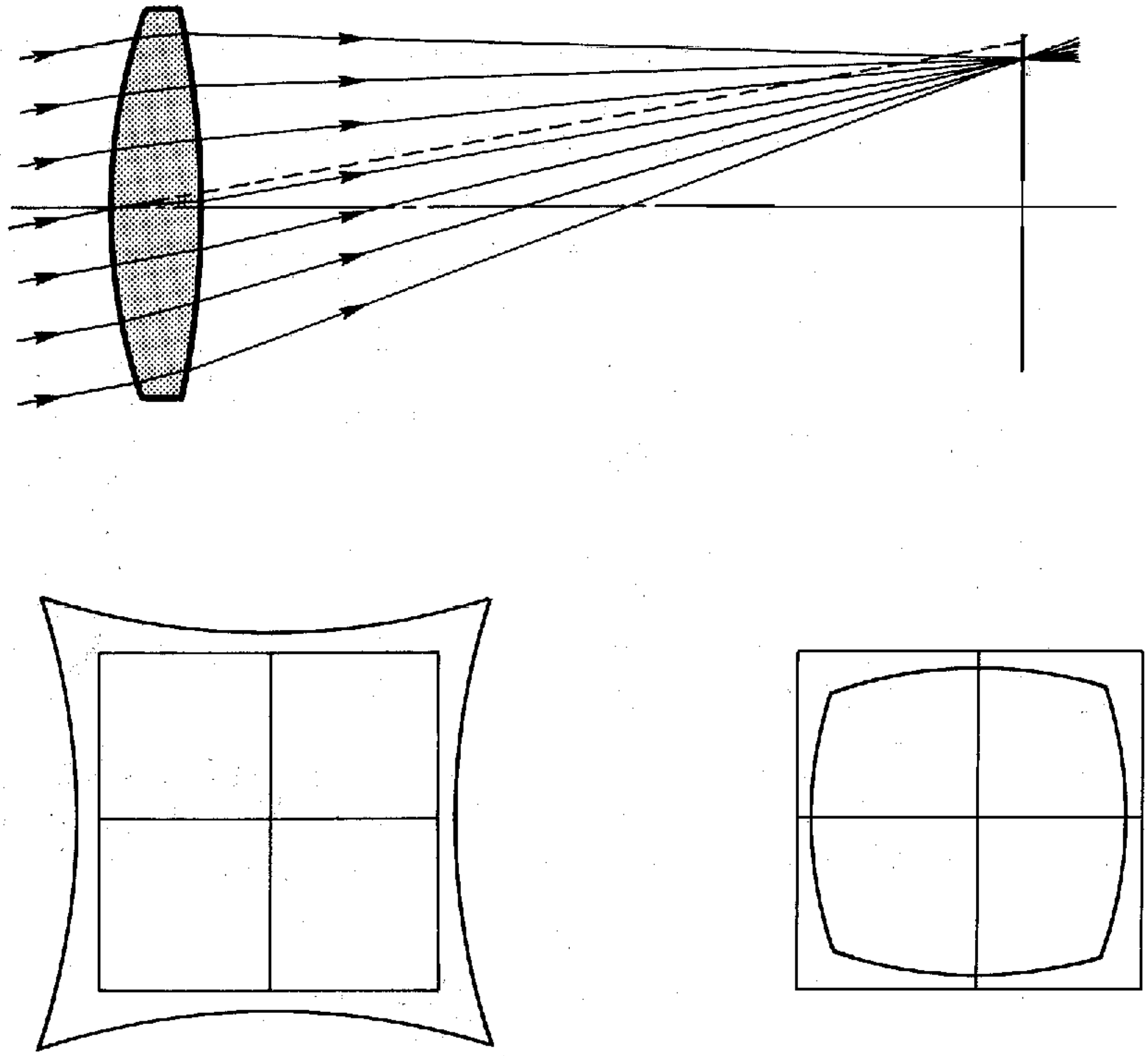

Figure 1: Ideal distortion pattern, from [Ruten & van Verrooij, 1988].
top: Optical geometry of a negative distortion. dashed line : ideal light ray going through the lens optical center. solid line : real distorded light rays. The real rays do converge, but not at the ideal position.
left: image deformation for positive distortion, called 'pincushion'.
right: image deformation for negative distortion, called 'barrel'.

1.3 Measuring the field distortion in flight.

Pre-launch ground based measurement of field distortion have been performed at IAS using a simulator of a point source. Knowing the exact position of the source, the ideal (non distorded) position on the detector aray is computed while the real one is measured. The difference between the two position gives the distortion in the system.

The same idea can be applied for in-flight measurement of the distortion. Since we cannot move the source (*i.e.* a star!), we move the detector. This is what happens when observing with the raster mode, as explained in figures 2 and 3.

Figure 2 shows an ideal raster map of a point source. The various position of the array are drawn. The source is seen by different pixels of the detector in each of the pointings. Figure 3 presents the nine images of the same raster. The postion of the source is figured by a circle if there was no distortion, and by a dot in the case of a ideal pincushion. The two positions are the same when the source is seen by the center of the array: we are on the optical axis and no distortion is present in that case, as explained in previous section. If we measure this position and know precisely how ISOCAM moves on the sky during the raster, we are able to compute the ideal position for all the other pointings (it is a translation if the satellite roll does not change). The difference between the real measurement and the computed ideal position is only due to the distortion.

Therefore, the requirements for an observation to measure the distortion are:

1. the satellite pointing accuracy must be more precise than the precision to which distortion can be measured. In our case, the limiting factor for the distortion measurement is the precision in measuring the position of a star. Our technique reach a tenth of a pixel. The limiting factor on the satellite side is either the relative pointing accuracy (between two raster pointings) , or the pointing jitter.

2. the observation must allow to measure the distortion on the whole array for as many pixels as possible. This can be done in two ways :

   The distance between pointings is small (1 pixel) and the source is seen by all pixels: a 32x32 raster is wished. The observation is made on a star bright enough.

   The observation contains many stars, even for a raster with bigger steps. The requirement is that all stars must have been seen by the central part of the field in order to compute ideal positions.

The second criteria will never be exactly completed because the column 23 of the detector is dead and no measure can be done at this position. Moreover, some other pixels will not be mapped, because the star did not fell on it, or because the pointing was lost due to glitches for example. Therefore, we will end the mesurement with a non homogeneous map of the field of view distortion of a given configuration. We will show in section 3.1 how to deal with such measurements.

The observations that matches these criteria are not very numerous, and careful checks of the pointing accuracy have to be made before attempting the measurements.

All this work is based on the ability to measure the position of a star on the detector array with a subpixel precision. We will now investigate various methods to reach this goal.

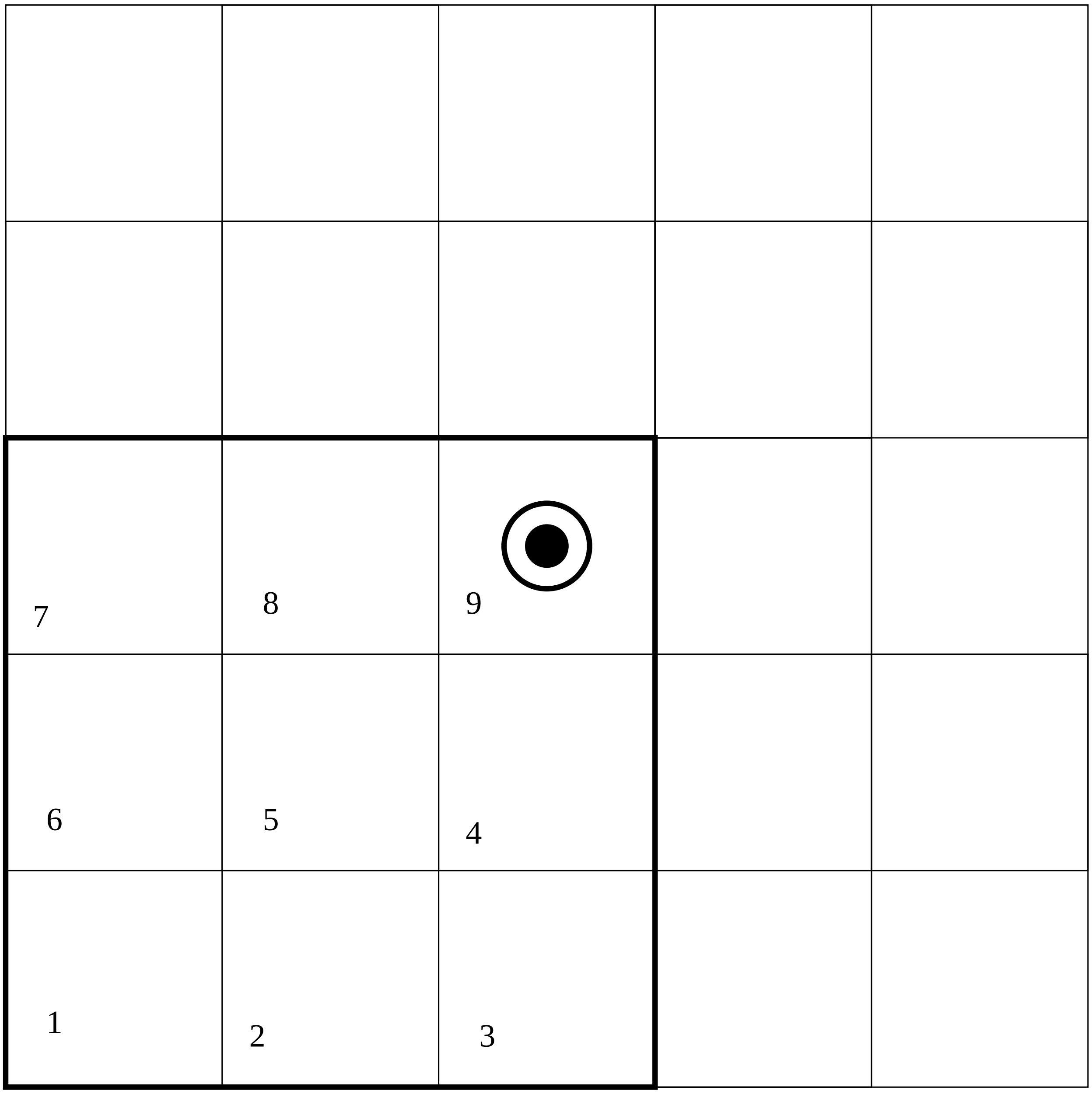

Figure 2: Ideal raster observation of a point source. The observation is a 3x3raster, the step being 1/3 of array in both axis. The nine raster position are numbered on their lower left corner. The first position is drawn with thick line.

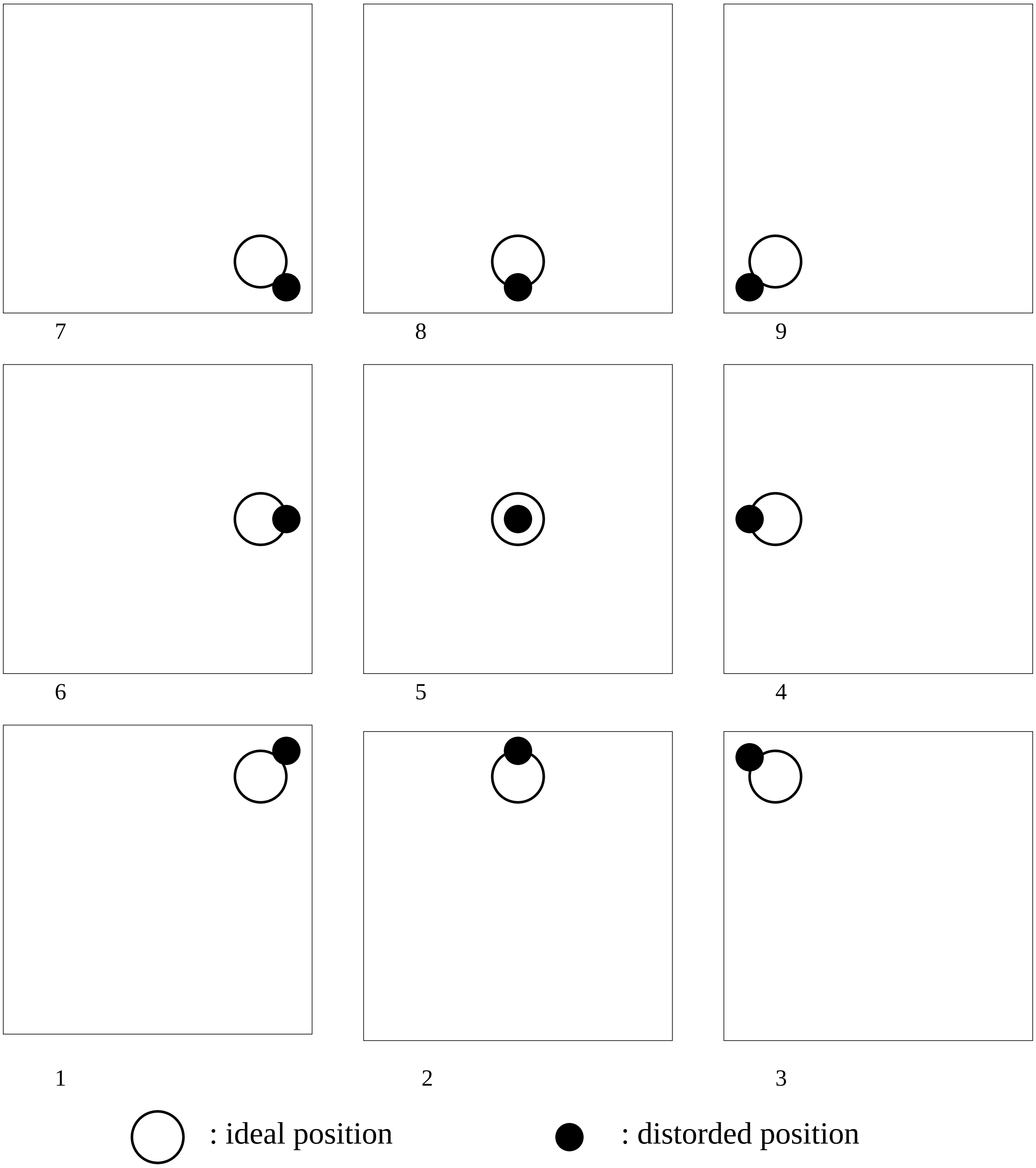

Figure 3: Distorded raster observation of a point source. The observation is a 3x3raster, the step being 1/3 of array in both axis. The nine raster position are numbered on their lower left corner.

2 Star position measurement

ISOCAM point spread function is severly undersampled by its detectors (SW and LW). The distortion effect was predicted to be rather small, *i.e.* smaller than a pixel on most of the array. We must derive a method that allow for the measure of the position of a point source (a star) on the array with a sub-pixel precision, ideally a tenth of a pixel.

Four methods to measure the position of a star on the array have been tested. They are:

1. the barycenter of the light.
2. DAOPHOT method, the *CNTRD* routine of the astronomical library.
3. fit of gaussian along the x and y axis through the star brightest pixel.
4. fit of the theoretical point spread function (PSF).

A well position controlled sample of stars is needed in order to test these method. Unfortunateley, due to ISO pointing accuracy (of the order of 6") and due the distortion, that displaces sources on the array, such sample does not exist. We use instead simulations of point sources. The point source can be modeled with the real ISOCAM PSF model [K. Okumura, 1997] that is discussed in appendix A. Important parameters is the signal over noise (S/N) ratio of the observation, and the size of the PSF. For each measurment method, we performed the following simulations :

- a point source image is modeled at a given position, using a modeled PSF.
- the star is moved in pixel (16,16) from the lower right corner of the pixel at position (15.5,15.5) to the upper left corner of the pixel at position (16.5,16.5). The position (16.0,16.0) indicates that the source is exactly centered on the pixel. This results in N simulations.
- the simulations are performed for total flux in the PSF of 10000, 1000, 100 and 20 ADU.
- a gaussian noise of 1 ADU is added to the simulated image.
- 100 simulations are performed per position and S/N.
- simulations are done for wavelength of 15 μm and 6.5 μm, as well as for broad band filters LW2 and LW3, with PFOV of 6" and 1.5".

This set of simulations enable us to discuss the efficiency of the four methods in recovering the input star positions.

2.1 Barycenter of the light

The baycenter of light of a star (point source) is the barycenter of the pixels illuminated by the point source, using the received flux as weight. Given a box around the point source, usually centered on the brightest pixel, the barycenter coordinates are :

$$x_B = \sum_{p \in box} x_p F_p / \sum_{p \in box} F_p \tag{1}$$

$$y_B = \sum_{p \in box} y_p F_p / \sum_{p \in box} F_p \tag{2}$$

where p is a pixel of the box, x_p and y_p its coordinates in pixels, F_p its flux.

This method has several drawbacks. All the flux received from the source should be in the box. If not, the box should not introduce any asymetry in the measurement of the flux: for exemple if the box contains only a part of the first airy ring. Therefore, this method cannot be used on the edges of the array. Unfortunately, that is where the effect of the distortion should be the largest. Moreover, the method is not precise, especially when the source is not centered on a pixel. Figure 4 illustrate the ability of this method to recover the position of a star observed.

For bright stars, the method appear biased toward the center of the pixel. The method find a wrong position, but with a very small rms, except at 3" PFOV. For fainter objects, the method fail in determining accurately the position of the input star, because the bias is larger and the precision is poorer. This method is not enough accurate to serve our purpose.

2.2 *CNTRD* routine

The *CNTRD* routine is part of IDL Astronomical library. It implements the DAOPHOT IRAF package task *daofind*, that is based on second order gaussian fit.

As for the barycenter, the *CNTRD* routine is biased for high fluxes, and even less acurate for faint sources (figure 5). This method should also not be used for our purposes.

2.3 Fit of gaussian

An other way to determine the position of star is to fit a gaussian profile along the X and Y axis of the image, through the brightest pixel. The *gaussfit* IDL routine can perform this task. However this function fits the sum of a polynomial and a gaussian function that can cause the program to run without finding any solutions. Moreover, if the source is near the edges of the array, it can be detected as an absorption pattern rather than an emission. For these reason, we designed a function, *gaussfit_psf*, that allows only for emission peak to be fitted, with a function of the form :

$$f = a_0 e^{-\frac{z^2}{2}} + a_3 + a_4 p + a_5 p^2 \tag{3}$$

with z defined with :

$$z = \frac{p - a_1}{a_2} \tag{4}$$

where a_1 is the position of the source along the axis. We use a non linear least square fit (IDL *curvefit*) as *gaussfit*. If this fails to cenverge (as it happen when the source is near the edges), we perform a simplex minimization with the condition :

$$a_4 = a_5 = 0 \tag{5}$$

Once the fit is done, a check can be done on the result, using the computed parameters to derive the flux F and full width half maximum W (FWHM) of the PSF, using the relations :

$$F = 2\pi a_0 a_2^2 \tag{6}$$

$$W = 2a_2\sqrt{2ln2} \tag{7}$$

The same test as for barycenter can be performed for this method. The result are shown on figure 6. The method works very well on bright 100 ADU source, with an average error of $\sigma = 0.04$ pixel. No hysteresis effect is found on the edge of the pixel. The average error for fainter sources (20 ADU) is $\sigma = 0.17$ pixel. Here again no hysteresis effect toward the center of the pixel is found. However, the precision acheived by the method in this case might not be sufficiebt for our purpose, as we see below.

2.4 Fit of PSF

It has been shown by [K. Okumura, 1997] that the theoretical model for ISOCAM PSF, which take into account the circular aperture, the central obscuration and the tripod structure, matches very well the observed PSF. Unfortunately, the model beeing computed through convolution in Fourier space, no algebraic formula is available to compute the theoretical PSF, given the position of a point source on the array.

We have computed sets of PSF, for each filter and lens of the LW channel, the point source being displaced inside the central pixel, by tenth of pixels, using an adaptated version the program *th_psf* by K. okumura and M. Perraut. We use the FITS convention, the central position of a pixel beeing the interger one. For each ISOCAM configuration, we have a set of N images of a theoretical PSF whose center sweep the range $[15.5, 16.5]$ both along X and Y axis, with steps of $1/\sqrt{N}$ pixel (see appendixA).

It is possible to recover the position of a source on the array, using these templates. We first look for the brightest pixel of the source. Then, we translate the N PSF from pixel (16,16) to this position. According to wavelength, we take a subimage containing the central core of the PSF[2]. We try to minimize the functionnal f_{PSF_n} of the n^{th} PSF on this subimage:

$$f_{PSF_n}(\alpha, \beta) = \sum_{i \in subima} (m_i - (\alpha p_i + \beta))^2 \tag{8}$$

where m_i is the measured flux in pixel i, p_i the flux in the PSF pixel i. α is the flux of the source while β is a constant background.

The differential of f_{PSF_n} is :

$$df_{PSF_n} = -2 \sum_{i \in subima} (m_i - (\alpha p_i + \beta))(p_i d\alpha + d\beta) \tag{9}$$

[2]The PSF model works well on the central core, but fails to account for non-symetrical patterns on the Airy rings [K. Okumura, 1997]

The condition for f to reach minimum is :

$$\frac{\partial f}{\partial \alpha} = \frac{\partial f}{\partial \beta} = 0 \tag{10}$$

This gives a 2 equation system with 2 unknown :

$$\sum_{i \in subima} p_i(m_i - \alpha p_i - \beta) = 0 \tag{11}$$

$$\sum_{i \in subima} (m_i - \alpha p_i - \beta) = 0 \tag{12}$$

The solution for α and β are :

$$\alpha = \frac{N \sum p_i m_i - \sum m_i \sum p_i}{N \sum p_i^2 - \sum p_i \sum p_i} \tag{13}$$

$$\beta = \frac{\sum p_i^2 \sum m_i - \sum p_i m_i \sum p_i}{N \sum p_i^2 - \sum p_i \sum p_i} \tag{14}$$

Where N is the number of pixels in subima.

The source flux α and the background β minimize the functional f_{PSF_n}, which is a distance between the measured source and the theoretical model. Having calculated them for all the N PSF, the one that matches the better the measure is given by :

$$n \in PSF \mid f_{PSF_n} = min\{f_{PSF}\} \tag{15}$$

that is the PSF that is the closer to the measure. This derivation is like a least square fit method, except that it is performed on discrete computed value of a more general unknown function that would give the PSF for any position in the pixel.

Since we simulate point source using theoretical PSF, a test like the one performed for barycenter and gaussian fit is not very interesting. However, it allows to check for the dependency with noise. The results are shown in figure 7. This shows clearly that for bright and faint source, the method gives good results, the average error for the 20 ADU source is $\sigma = 0.11$ pixel. Nevertheless, for real source, the position will not be exactly a tenth of a pixel, so the precisin of the method is no less than 0.1 pixel.

This method has three great advantages :

1. the flux and background being derived during the minimization, they are available for constitency checks.

2. it runs faster than the gaussian fit.

3. the method works well with sources that are near the edges of the array, while the gaussian fit fails because of the lack of points. This is illustrated on figure 8 where a 50 ADU source is displaced in pixel (1,1). The distortion effect is bigger on the edge so this property is very interesting.

It has been pointed out by [K. Okumura, 1997] that the measured PSFs show a little asymetry on the first Airy ring. The concerned flux are very low: less than 3% of the total flux. Moreover, we perform our fit mainly on the central core of the PSF, where the theoretical model matches very well the measurement. This should ensure that the method is reliable.

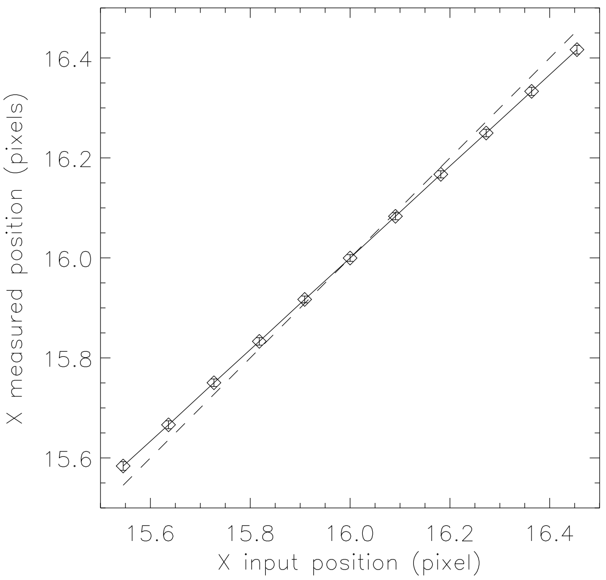

(a) Simulation with 1.5" PFOV, LW3. Measured X position of a 10000 ADU star over a 1 ADU noise *vs.* the input X position.

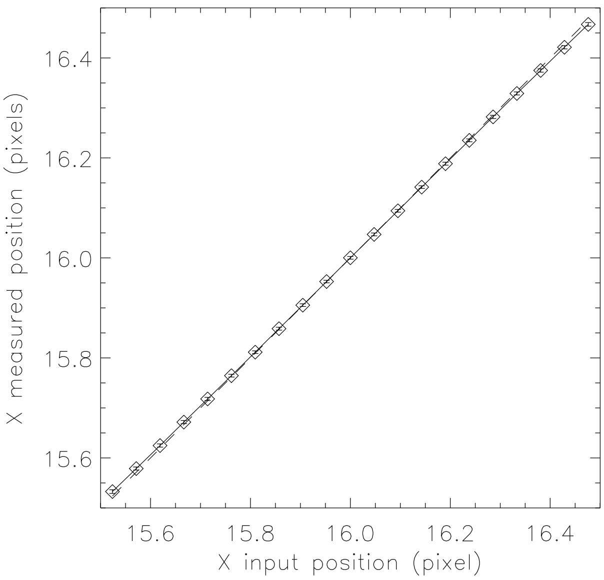

(b) Simulation with 3" PFOV, LW3. Measured X position of a 10000 ADU star over a 1 ADU noise *vs.* the input X position.

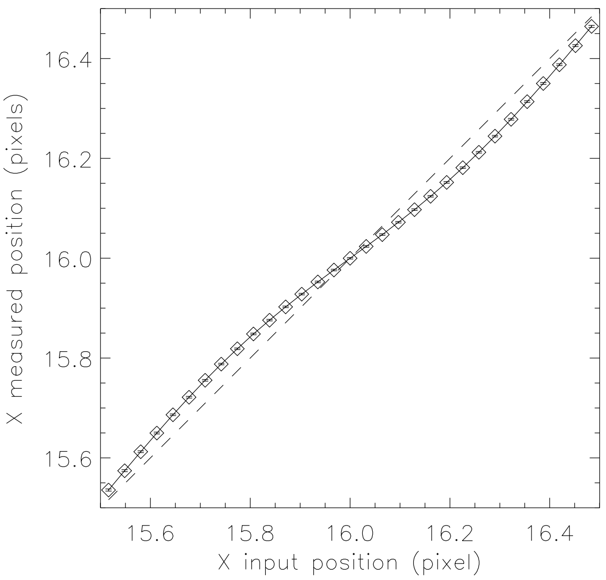

(c) Simulation with 6" PFOV, LW3. Measured X position of a 10000 ADU star over a 1 ADU noise *vs.* the input X position.

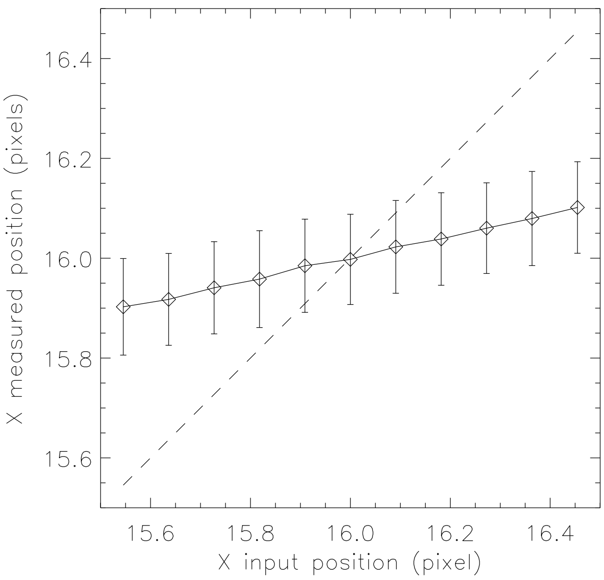

(d) Simulation with 1.5" PFOV, LW2.Measured Y position of a 100 ADU star over a 1 ADU noise *vs.* the input Y position.

Figure 4: Measurement of the position of a simulated star with LW3 filter, using the barycenter method. Input star was simulated at each position allowed by the theoretical PSF. Integer position *i.e.* $x = 16.0$ and $y = 16.0$ indicate that the star is exactly centered in the pixel. The barycenter was computed over a box enclosing the central peak of the PSF for ech PFOV.

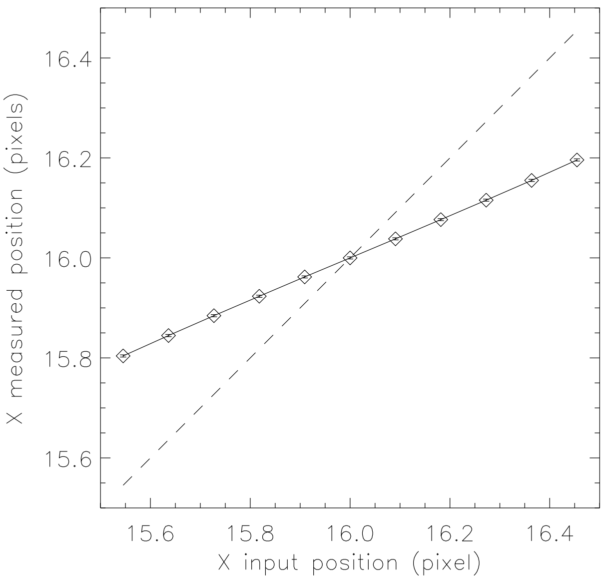

(a) Simulation with 1.5" PFOV, LW3. Measured X position of a 10000 ADU star over a 1 ADU noise *vs.* the input X position.

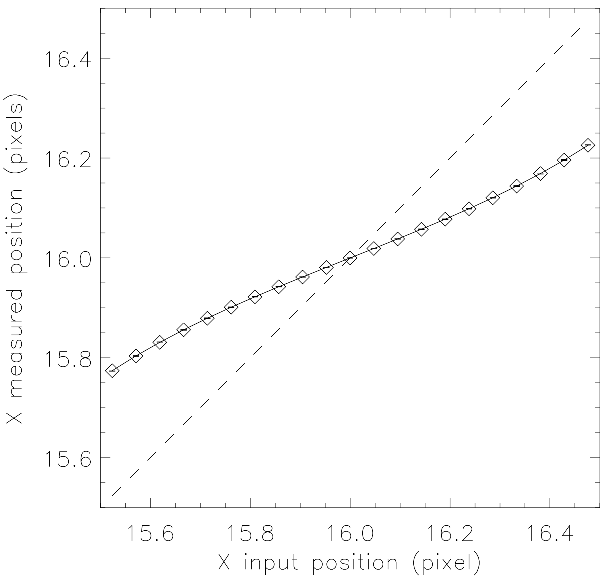

(b) Simulation with 3" PFOV, LW3. Measured X position of a 10000 ADU star over a 1 ADU noise *vs.* the input X position.

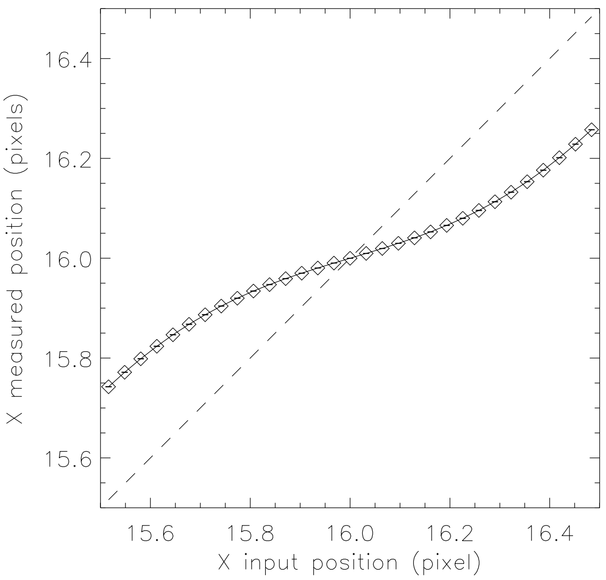

(c) Simulation with 6" PFOV, LW3. Measured X position of a 10000 ADU star over a 1 ADU noise *vs.* the input X position.

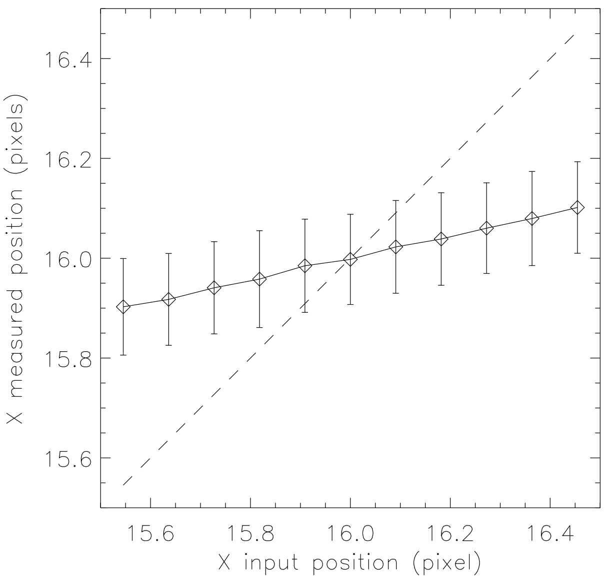

(d) Simulation with 1.5" PFOV, LW2.Measured Y position of a 100 ADU star over a 1 ADU noise *vs.* the input Y position.

Figure 5: Measurement of the position of a simulated star with LW3 filter, using the *CNTRD* routine. Input star was simulated at each position allowed by the theoretical PSF. Integer position *i.e.* $x = 16.0$ and $y = 16.0$ indicate that the star is exactly centered in the pixel. The full width half maximum was given for each PFOV to the routine.

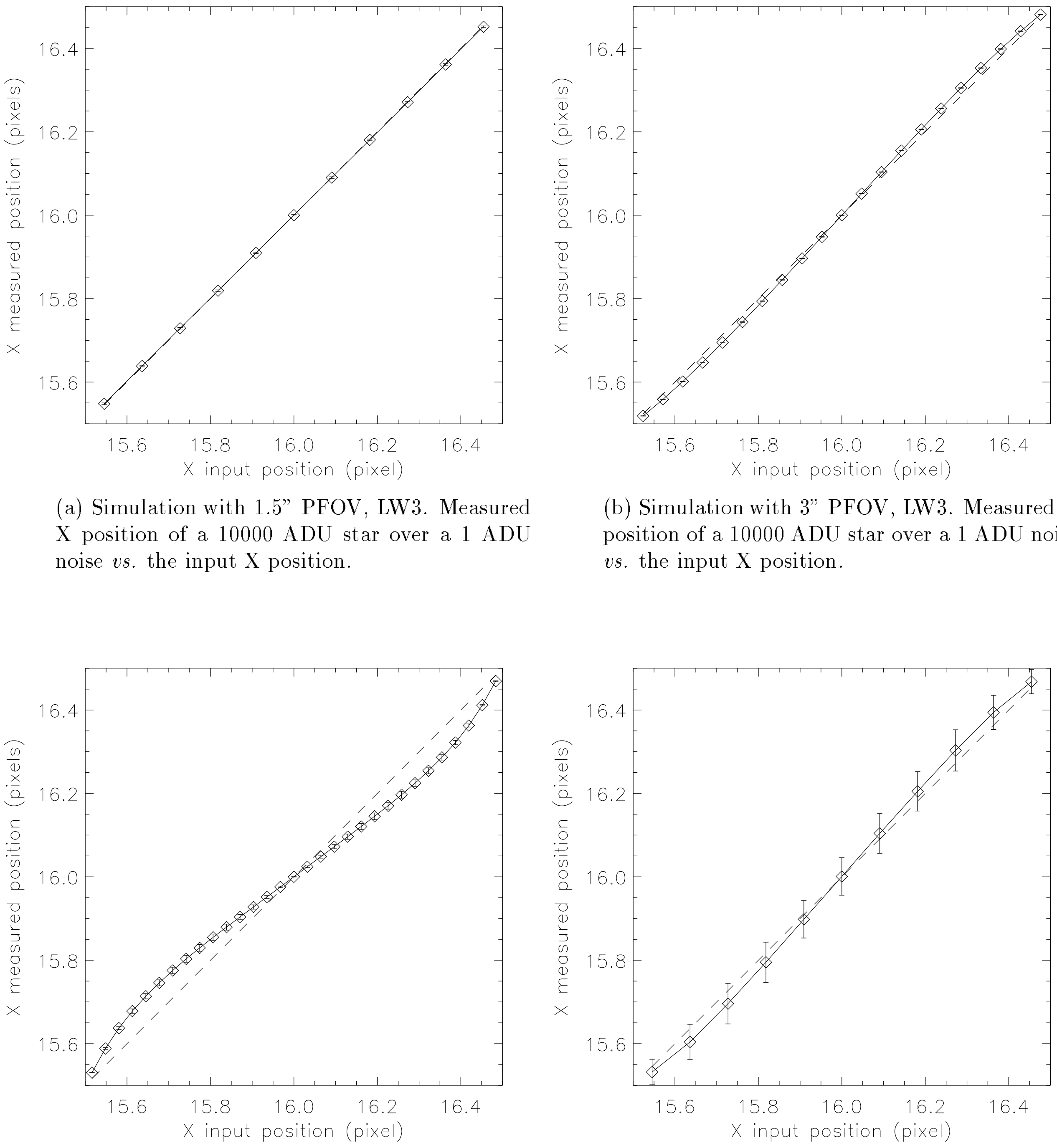

(a) Simulation with 1.5" PFOV, LW3. Measured X position of a 10000 ADU star over a 1 ADU noise *vs.* the input X position.

(b) Simulation with 3" PFOV, LW3. Measured X position of a 10000 ADU star over a 1 ADU noise *vs.* the input X position.

(c) Simulation with 6" PFOV, LW3. Measured X position of a 10000 ADU star over a 1 ADU noise *vs.* the input X position.

(d) Simulation with 1.5" PFOV, LW2.Measured Y position of a 100 ADU star over a 1 ADU noise *vs.* the input Y position.

Figure 6: Measurement of the position of a simulated star with LW3 filter, using fit of gaussian. Input star was simulated at each position allowed by the theoretical PSF. Integer position *i.e.* $x = 16.0$ and $y = 16.0$ indicate that the star is exactly centered in the pixel.

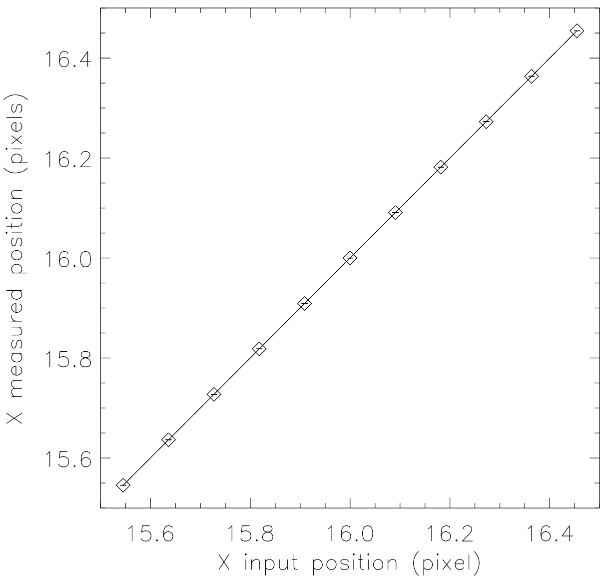

(a) Simulation with 1.5" PFOV, LW3. Measured X position of a 10000 ADU star over a 1 ADU noise *vs.* the input X position.

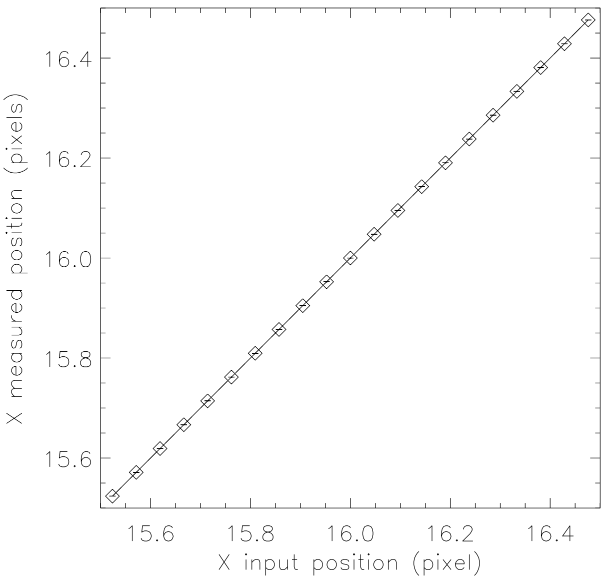

(b) Simulation with 3" PFOV, LW3. Measured X position of a 10000 ADU star over a 1 ADU noise *vs.* the input X position.

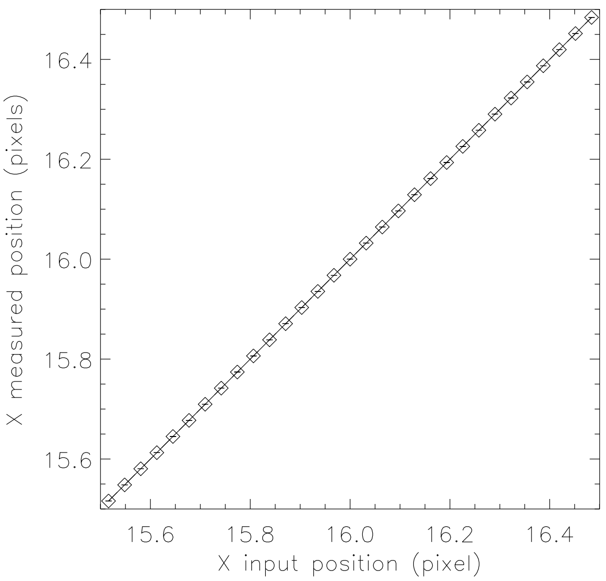

(c) Simulation with 6" PFOV, LW3. Measured X position of a 10000 ADU star over a 1 ADU noise *vs.* the input X position.

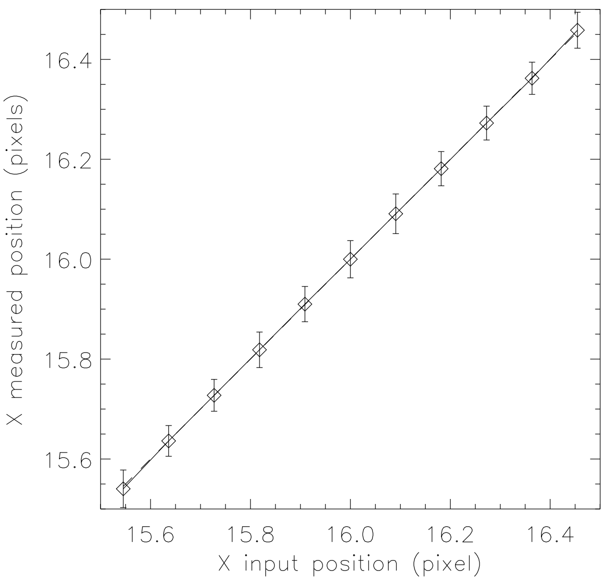

(d) Simulation with 1.5" PFOV, LW2.Measured Y position of a 100 ADU star over a 1 ADU noise *vs.* the input Y position.

Figure 7: Measurement of the position of a simulated star with LW3 filter, using fit of PSF. Input star was simulated at each position allowed by the theoretical PSF. Integer position *i.e.* $x = 16.0$ and $y = 16.0$ indicate that the star is exactly centered in the pixel.

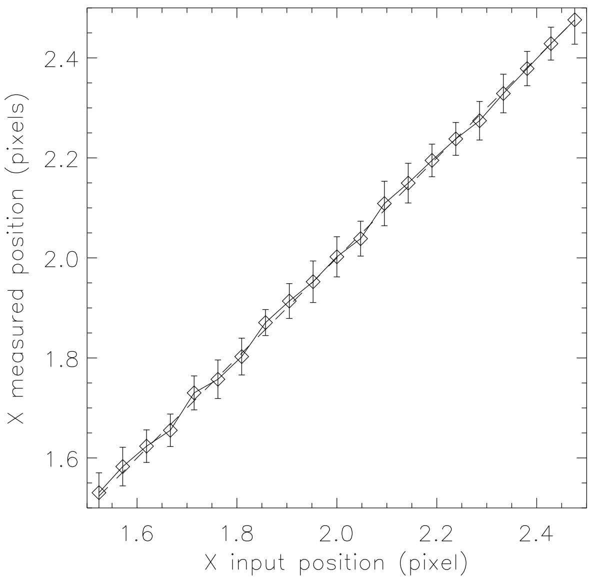

(a) Simulation with 3" PFOV, LW3. Measured X position of a 100 ADU star in pixel(2,2) over a 1 ADU noise *vs.* the input X position using a fit of PSF.

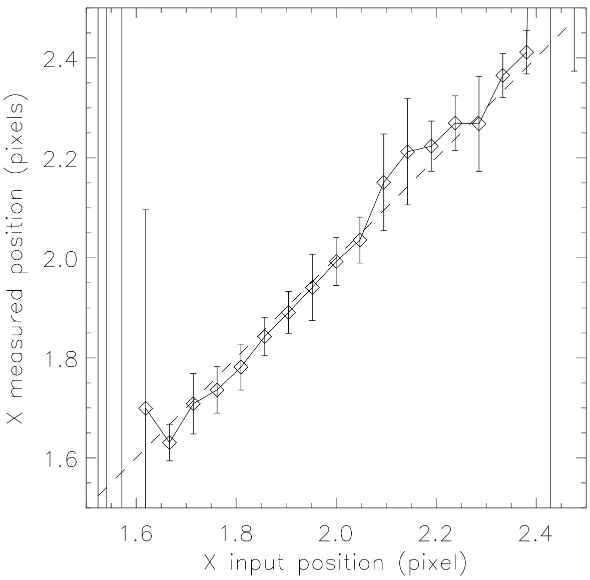

(b) Simulation with 3" PFOV, LW3. Measured X position of a 100 ADU star in pixel(2,2) over a 1 ADU noise *vs.* the input X position using a fit of gaussian.

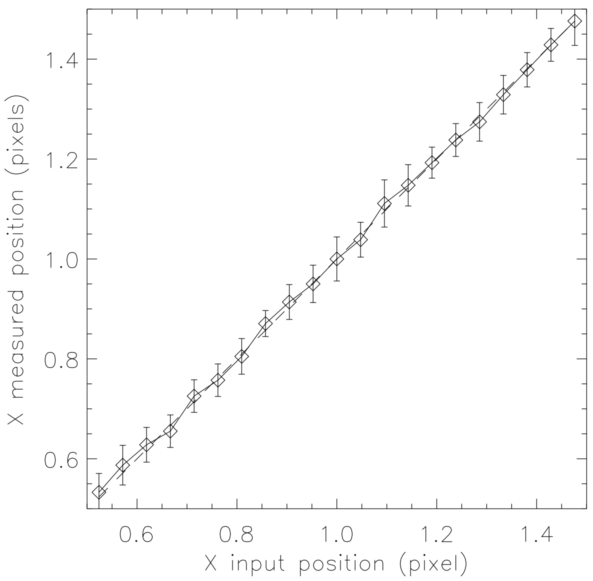

(c) Simulation with 3" PFOV, LW3. Measured X position of a 100 ADU star in pixel (1,1) over a 1 ADU noise *vs.* the input X position using a fit of PSF.

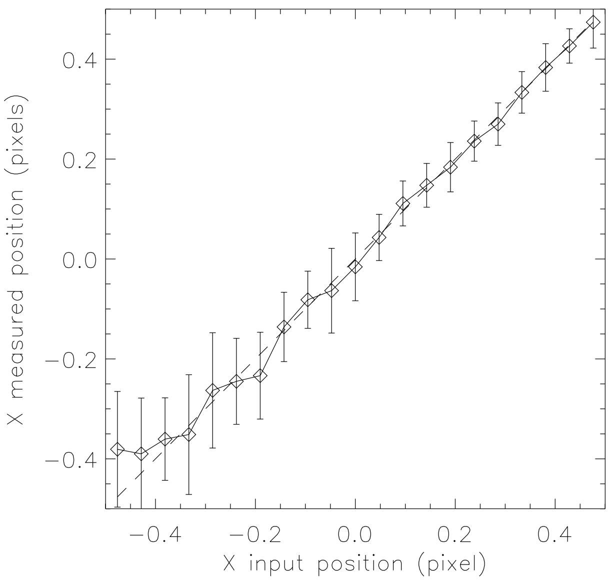

(d) Simulation with 3" PFOV, LW3.Measured Y position of a 100 ADU star in pixel (0,0) over a 1 ADU noise *vs.* the input Y positionusing a fit of PSF.

Figure 8: Comparison of the efficiency of the fit of PSF and the fit of gaussian, when the star is near the edges of the array (a et b). PSF fit allow to fit postion with good precision even in pixel (1,1) (c) or (0,0) (d).

PFOV	LW1	LW2	LW3	LW4	LW5	LW6	LW7	LW8	LW9	LW10
1.5"	0.42	0.26	0.07	0.29	0.23	0.19	0.13	0.10	0.06	0.11
3"	0.62	0.55	0.22	0.58	0.54	0.49	0.39	0.31	0.20	0.33
6"	0.82	0.69	0.52	0.71	0.66	0.63	0.61	0.60	0.50	0.59

Table 2: Percentage of light received by the brigthest pixel of a PSF (for a star at the center of the pixel), with respect to the total light received by the detector array

2.5 Measurement of the position of a star

Comparing the various method show that some are biased, and that their precision depends on the observation S/N. More precisely, the important parameter is not the global S/N, but the S/N in the brigthest pixel. Table 2 displays the percentage of light that is seen in the brightest pixel as a function of the PFOV and the filter. In respect with this parameter, our figures 4, 5, 6 and 7 show four tests made with a S/N of 700 at 1.5",LW3 , and 26 at 1.5", LW2. These S/N are rather high. However barycenter and *CNTRD* fail in the last case.

Of the four techniques that were tested, only the fit of theoretical PSF has proven to work effeciently for a wide range of S/N, and on the edges of the array. Its precision is for most cases fixed by the method itself that sample PSF by tenth of pixels. For bright sources, the gaussian method that reaches 0.01 pixels is more precise, if corrected for its bias, because working on continous functions. For these reasons, we have derived the following policy for the star position measurement :

- Bright sources: gaussian and fit of PSF are performed. If both agree when gaussian fit is corrected for its bias, this one is used. If the two disagree, often because the source is at the edges of the array, the PSF fit is used. In any case, the flux measurement are recorded for constitency checks.
- Faint sources: the PSF fit is used. The flux measurement are recorded for constitency checks.

3 Distortion correction.

Once the distortion has been mapped for a given ISOCAM configuration, the information can be used to correct the observation in the same configuration. Since the mapping is not perfect, we fit it with analytical functions, in order to be able to apply it on the whole array.

3.1 fitting the distortion map.

The distortion map is fitted by a general polynomial of degree 3, following the work done for the HST WFPC2 calibration [Holtzman et al., 1997].

$$x_m = a_0 + a_1x_c + a_2y_c + a_3x_c^2 + a_4x_cy_c + a_5y_c^2 + a_6x_c^3 + a_7x_c^2y_c + a_8x_cy_c^2 + a_9y_c^3 \tag{16}$$

$$y_m = b_0 + b_1x_c + b_2y_c + b_3x_c^2 + b_4x_cy_c + b_5y_c^2 + b_6x_c^3 + b_7x_c^2y_c + b_8x_cy_c^2 + b_9y_c^3 \tag{17}$$

Where x_m and y_m are the measured distorded positions while x_c and y_c are the non distorded ones. The fit of the a_i and b_i is done by orthogonally projecting the overdeterminated system obtained from the measurements on the on the basis a_i and b_i, using the IDL routine *SVDC*. This minimizes the system in the sense of least-squares.

For correction purpose, we need to be able to compute x_c and y_c, knowing x_m and y_m. Following again the work from WFPC2 calibration [Holtzman et al., 1997], we fit again a general polynomial of degree 3 rather than computing directly the inversion of equations 16 and 17. We have :

$$x_c = c_0 + c_1 x_m + c_2 y_m + c_3 x_m^2 + c_4 x_m y_m + c_5 y_m^2 + c_6 x_m^3 + c_7 x_m^2 y_m + c_8 x_m y_m^2 + c_9 y_m^3 \quad (18)$$

$$y_c = d_0 + d_1 x_m + d_2 y_m + d_3 x_m^2 + d_4 x_m y_m + d_5 y_m^2 + d_6 x_m^3 + d_7 x_m^2 y_m + d_8 x_m y_m^2 + d_9 y_m^3 \quad (19)$$

Equations 18 and 19 allow us to compute the non distorded position of a pixel on the array, *i.e.* where its projection on the sky lies.

3.2 Projection on the sky

It is obvious from equations 18 and 19 that ISOCAM pixel is no more a square. This has to be taken into account when reconstructing raster maps and projecting on the sky. Moreover, the area covered by each pixel on the sky is no more constant through the array. We have designed a program that perform flux conservative projection on the sky, using FITS files as input, called *projection*.

In order to take into account the difference of pixel surface, we first have to correct the flat-fielding of ISOCAM images. The usual flat-field is computed assuming that ISOCAM sees a constant background (i. e. a flat field). The distortion makes this assumption false. The images have to be divided by a new flat, F_D that will correct for this effect. Since the central pixel is the less distorded, we have :

$$F_{i,j} = \frac{S_{16,16}}{S_{i,j}} \quad (20)$$

with $S_{i,j}$ is the surface on the sky of pixel i,j.

Once this correction is made, we do for each pixel of the image:

1. compute the distortion-free pixel coordinates of its corner, using equations 18 and 19
2. compute the R.A. and Dec of the corners using the RA-TAN and DEC-TAN projection.
3. compute the pixels coordinates of the corners in the raster map, using the reverse RA-TAN and DEC-TAN projection.
4. compute the area of the intersection of the pixel with each pixel of the raster map it falls on, using the same algorithm as [Fruchter et al., 1997] in their *drizzle* IRAF task.
5. add to the raster map pixels the value of the input pixel times the ratio of the intersecting surface to the input surface.

The raster map is constructed following this shift and add algorithm. Hence, we have:

$$R_{x,y} = \frac{\sum_{pointings} S_{(x,y,i,j)} \sqrt{N_{i,j}} I_{i,j}}{\sum_{pointings} S_{(x,y,i,j)} \sqrt{N_{i,j}}} \tag{21}$$

Assuming gaussian distributions for pixels, the noise map is:

$$\sigma_{x,y} = \sqrt{\frac{\sum_{pointings} S^2_{(x,y,i,j)} N_{i,j} \sigma^2_{i,j}}{\sum_{pointings} S^2_{(x,y,i,j)} N_{i,j}}} \tag{22}$$

Where $R_{x,y}$ is the value of the final raster map at (x,y), $S_{(x,y,i,j)}$ is the intercepted surface between ISOCAM pixel (i,j) and raster map pixel (x,y) and $N_{i,j}$is the number of readouts that where averaged together to produce $I_{i,j}$, the image of the raster pointing.

The final raster image, $R_{x,y}$, is corrected for distortion.

4 LW 6" PFOV distortion

Since the 6" pixel field of view lens sample the largest field, it is waited that its distortion should be the most important.

4.1 Available observations

4.2 GRB rasters 1 and 2 measurement

4.3 GRB rasters 3 and 4 measurement

4.4 The lens jitter problem

4.5 Polynomial coefficients

4.6 Cluster measurement

4.7 Conclusion for the 6" lens

5 LW 3" PFOV distortion

5.1 Available observations

5.2 GRB measurement

5.3 Cluster measurement

5.4 Conclusion for the 3" lens

5.5 LW 1.5" PFOV distortion

5.6 Available observations

5.7 Cluster measurement : the satellite jitter

5.8 Conclusion for the 1.5" lens

6 Improvements of the distortion correction

7 Conclusion

References

[Fruchter et al., 1997] Fruchter A.S., Hook R.N., 1997 , *http://www.stsci.edu/ fruchter/dither/drizzle.html*

[Holtzman et al., 1997] Holtzman J. et al., 1997, PASP , 107, 156

[Icenogle et al., 1976] H. W. Icenogle et al., Applied Optics, 15, 10, pp 2348, 1976.

[Lena, 1988] P. Lena, Observational astrophysics, 1988 , Springer-Verlag.

[K. Okumura, 1997] K. Okumura, ISOCAM PSF Report, September 5, 1997, *http://isowww.estec.esa.nl/instr/CAM/cal_wksp/psf_report.ps.gz*

[Ruten & van Verrooij, 1988] H. Rutten, M. van Venrooij, Telescope optics, a comprehensive manual for amateur astronomers, 1988, Willmann-Bell.

A The ISOCAM PSF model

The ISOCAM PSF model has been developped by M. Perraut and K. Okumura [K. Okumura, 1997] and I recall here its main properties only.

The PSF at a single wavelength is computed by convolving a point source by the ISO aperture. ISO being a Cassegrain telescope, its optical parameters are :

1. The aperture of ISO : a circular primary mirror of 60 cm of diameter.
2. The circular hole in the primary miror, of 17.4 cm of diameter. The secondary miror is omitted because it is masked by the hole.
3. The tripod holding the secondary mirror : the width of the three arms is 2 cm.

The computation is directly made in Fourier space, on a grid of dimensions NxN where N is a power of two. The real image is then computed using a fast fourier transform (FFT). This image is integrated over ISOCAM dectector pixels.

The PSF image is computed with the desired angular resolution. However, in fourier space, the radius R^* of the aperture is given by :

$$R^* = \frac{RNs}{\lambda} \tag{23}$$

where R is the radius of the aperture, s the resolution in arcsec and λ the wavelength. To reach a sufficient presision, s has to be small*vs* the PFOV, and R^* has to be large to allow to draw a nice circle in the aperture image. The only way to combine the two constraints is to have N large. For this reason, the main limitation is the memory and speed of the computer. Our PSF have been computed on 2048x2048 grid, leading us to have at least 11x11 points in the PSF image for one ISOCAM pixel at 1.5" PFOV, with an aperture radius greater than 30 pixels in fourier space.

PSF for a single wavelength where computed from 4 μm to 18 μm, by step of 0.5 μm. These PSF match well CVF observations. The PSF of broad band filters where computed by adding these PSF, weighted by the transmission curve of the filters given in the LWSPEC calg. For exemple, the LW5 PSF is obtained by :

$$P_{LW5} = P_{6.5\mu m} \int_{6.25}^{6.75} T_{LW9}(\lambda) d\lambda + P_{7.0\mu m} \int_{6.75}^{7.25} T_{LW9}(\lambda) d\lambda \tag{24}$$

Where T_{LW9} is the transmission of the LW9 filter.

All the PSF are normalized so that their integral over the LW detector array is 1.

B Measurements

This appendix is organized as follow. For each observation used to measure the distortion, a table gives the following informations :

1. General information :

   TDT

   Proposal name

   Target

2. Configuration

   Lens (pixel field of view)

   Lens position (*cf* lens jitter) if the background is sufficient to measure it.

   Filter

3. Raster parameters

   number of steps

   step size between pointings

4. Measurement information

   Number of object used

   Average S/N on the brightest pixel

   flux of the star

   background level

   average number of measurement point per object (some raster positions may be lost)

   total number of point used

   average residual in arcsec between theoretical and observed positions

   average residual in arcsec between theoretical and corrected positions

5. the polynom

B.1 PFOV = 6"

B.1.1 Observation of the LW3 ghost

TDT:	576007001	PFOV:	6”
Proposal:	GHOSTLW	Lens Position:	left
Target:	HIC87585	Filter:	LW3
Raster:	9x9	Number of stars	1
N Raster Step:	21”	Average flux:	15343 ADU/G/s
M Raster Step:	21”	Background:	
Total Number of points:	81	S/N:	254
original residual:	1.54”/point	corrected residual	0.05”/point

c_0 1.294×10^{0}	c_1 9.124×10^{-1}	c_2 -6.938×10^{-2}	c_3 6.088×10^{-4}	c_4 3.999×10^{-3}
c_5 7.545×10^{-4}	c_6 -5.185×10^{-6}	c_7 -3.282×10^{-6}	c_8 -4.980×10^{-5}	c_9 1.534×10^{-6}
d_0 5.985×10^{-1}	d_1 7.149×10^{-3}	d_2 8.888×10^{-1}	d_3 4.971×10^{-5}	d_4 2.521×10^{-3}
d_5 3.537×10^{-3}	d_6 -8.063×10^{-6}	d_7 -7.234×10^{-5}	d_8 4.080×10^{-6}	d_9 -5.638×10^{-5}